

The brightest GRB ever detected: GRB 221009A as a highly luminous event at $z = 0.151$

D. B. Malesani^{1,2,3,*}, A. J. Levan^{1,4}, L. Izzo⁵, A. de Ugarte Postigo⁶, G. Ghirlanda^{7,8}, K. E. Heintz^{2,3},
D. A. Kann^{9,**}, G. P. Lamb¹⁰, J. Palmerio¹¹, O. S. Salafia⁷, R. Salvaterra¹², N. R. Tanvir¹³,
J. F. Agüí Fernández¹⁴, S. Campana⁷, A. A. Chrimes^{1,15}, P. D'Avanzo⁷, V. D'Elia¹⁶, M. Della Valle¹⁷,
M. De Pasquale¹⁸, J. P. U. Fynbo^{2,3}, N. Gaspari¹⁰, B. P. Gompertz¹⁹, D. H. Hartmann²⁰, J. Hjorth⁵,
P. Jakobsson²¹, E. Palazzi²², E. Pian²², G. Pugliese²³, M. E. Ravasio^{1,7}, A. Rossi²², A. Saccardi¹¹,
P. Schady²⁴, B. Schneider²⁵, J. Sollerman²⁶, R. L. C. Starling¹³, C. C. Thöne²⁷, A. J. van der Horst²⁸,
S. D. Vergani^{11,7}, D. Watson^{2,3}, K. Wiersema²⁹, D. Xu³⁰, T. Zafar³¹, and S. Y. Zheng^{2,3}

(Affiliations can be found after the references)

Received 15 February 2023 / Accepted 9 June 2024

ABSTRACT

Context. The extreme luminosity of gamma-ray bursts (GRBs) makes them powerful beacons, thus effective probes of the distant Universe. The most luminous bursts are typically detected at moderate and high redshift, where the volume for seeing such rare events is maximized and the star-formation activity is greater than at $z = 0$. For distant events, not all observations are feasible, such as those at TeV energies.

Aims. Here we present a spectroscopic redshift measurement for the exceptional GRB 221009A, the brightest GRB observed to date, with emission extending well into the TeV regime.

Methods. We used the X-shooter spectrograph at the ESO Very Large Telescope (VLT) to obtain simultaneous optical to near-infrared (NIR) spectroscopy of the burst afterglow 0.5 days after the explosion.

Results. The spectra exhibit both absorption and emission lines from material in a host galaxy at $z_{\text{GRB}} = 0.15095 \pm 0.00005$. Thus, GRB 221009A was a relatively nearby burst with a luminosity distance of $d_L = 745$ Mpc. Its host galaxy properties (star-formation rate and metallicity) are consistent with those of long GRB hosts at low redshift. This redshift measurement yields information on the energy of the burst. The inferred isotropic energy release, $E_{\text{iso}} > 5 \times 10^{54}$ erg, lies at the high end of the distribution, making GRB 221009A one of the nearest and also most energetic GRBs observed to date. We estimate that such a combination (nearby as well as intrinsically bright) occurs between once every few decades and once per millennium.

Key words. gamma-ray burst: general – gamma-ray burst: individual: GRB 221009A

1. Introduction

The population of so-called “long-duration” gamma-ray bursts (GRBs), which form via the collapse of massive stars and typically have prompt phase durations in the range of ~ 2 –1000 s, constitute the most luminous events in the known Universe (e.g., Kann et al. 2007; Racusin et al. 2008; Bloom et al. 2009; Frederiks et al. 2013). They have been detected from a redshift of as small as $z = 0.01$ (Galama et al. 1998) to $z = 8$ (Tanvir et al. 2009; Salvaterra et al. 2009; Tanvir et al. 2018) and possibly beyond $z = 9$ (Cucchiara et al. 2011). Their apparent isotropic-equivalent energies also span a large range. The observed local ($z \lesssim 0.2$) burst population is typically of low luminosity, with energies (assuming isotropic emission) of $E_{\text{iso}} \sim 10^{48}$ – 10^{50} erg (e.g., Soderberg et al. 2004). This reflects the fact that the space density of low-luminosity events is much higher than that of energetic ones. In contrast, at high redshift, we are able to sample a much larger volume, where the GRB rate is enhanced compared to the local Universe because of the increase in cosmic star formation. This allows us to detect those comparatively rare GRBs with an isotropic energy release that is higher by up to six orders of magnitude ($E_{\text{iso}} > 10^{54}$ erg; e.g., Cenko et al. 2011). The range of GRB luminosities reflects some observational effects, such as the angle between our line of sight and the axis of

the geometrically beamed relativistic jet, but it is also likely that the conditions of the progenitor star at the point of core collapse impact the properties of the subsequent GRB.

Studies of GRBs in the relatively local Universe are of particular value because their proximity offers diagnostics that are typically not available for the more distant events. For example, as the supernovae (SNe) associated with GRBs peak at much fainter magnitudes than the GRB afterglows themselves (especially in the UV), we can study the associated SNe in detail only at $z < 0.3$ (Hjorth & Bloom 2012; Cano et al. 2017; Schulze et al. 2014; D'Elia et al. 2015). Similarly, the lower luminosity distances and better spatial resolution enable studies of their host galaxies and underlying stellar populations in considerably greater detail (e.g., Izzo et al. 2017; Krühler et al. 2017; Tanga et al. 2018; de Ugarte Postigo et al. 2020).

Here we consider the case of GRB 221009A, the brightest GRB observed in over five decades of wide-field-of-view gamma-ray sky monitoring. The detection of TeV photons from this GRB (Dzhappuev et al. 2022; LHAASO Collaboration 2023; Cao et al. 2023) is also unprecedented, both in terms of their energy and flux, making the distance to this event of particular significance, because the mean free path of such photons is limited by their interactions with background light photons (Gilmore et al. 2012; Franceschini & Rodighiero 2017). Our X-shooter spectroscopy of the burst provides a robust redshift measurement of $z = 0.151$, consistent with being a cosmological

* Corresponding author: d.malesani@astro.ru.nl

** Deceased.

Table 1. Log of X-shooter spectroscopic observations.

Mid observing time (UT)	Time since GRB (days)	Exposure times (s)	Airmass	Seeing ($''$)	Slit widths ($''$)	Slit position angle (deg)
2022 Oct. 10.0504	0.498	4×600	1.8	0.85	1.0, 0.9, 0.9	146.7
2022 Oct. 20.0139	10.460	4×900 (VIS), 8×480 (NIR)	1.7	0.80	1.0, 0.9, 0.9	0.0

Notes. The second column shows the time since the *Fermi*/GBM trigger (2022 Oct. 9, 13:16:59 UT). The three slit widths refer to the UVB, VIS, and NIR arms, respectively, and the slit position angle is measured counterclockwise from North.

GRB and not a transient originating in the Milky Way (MW) as its location on the sky may suggest. The implied luminosity distance¹ of $d_L = 745$ Mpc places GRB 221009A amongst the most energetic GRBs ever observed, and makes it by far the closest GRB with $E_{\text{iso}} > 10^{54}$ erg.

2. Observations

2.1. High-energy discovery

GRB 221009A was detected at 2022 October 9 at 13:16:59 UT by a raft of high-energy missions including *Fermi*/GBM (Veres et al. 2022; Lesage et al. 2023), *Fermi*/LAT (Bissaldi et al. 2022), AGILE/MCAL and GRID (Ursi et al. 2022; Piano et al. 2022; Tavani et al. 2023), INTEGRAL (Gotz et al. 2022; Rodi & Ubertini 2023), Konus/Wind (Frederiks et al. 2022, 2023), INSIGHT/HMXT (Tan et al. 2022; Kann et al. 2023), STPSat-6/SIRI-2 (Mitchell et al. 2022), SATech-01/GECAM-C HEBS (Liu et al. 2022), SRG/ART-XC (Lapshov et al. 2022), Solar Orbiter/STIX (Xiao et al. 2022), and GRBalpha (Ripa et al. 2022; Řípa et al. 2023). However, the event was first reported by a *Swift* detection of the afterglow over 50 minutes later (Dichiara et al. 2022b). The location of the burst within the Galactic plane ($l = 52.96^\circ$, $b = 4.32^\circ$), combined with its brightness, led to confusion over the nature of the outburst: initially it was suspected to be due to a new Galactic X-ray transient (Dichiara et al. 2022b,a), but its subsequent behavior, together with the *Fermi*/GBM and LAT detections, appeared more like that of an extragalactic GRB (Kennea & Williams 2022; Veres et al. 2022; Bissaldi et al. 2022).

Despite high foreground extinction (Sect. 3.2), an optical afterglow was seen by various telescopes (e.g., Dichiara et al. 2022b; Lipunov et al. 2022; Fulton et al. 2023 and many more). The counterpart was localized at coordinates (J2000): RA = $19^{\text{h}}13^{\text{m}}03^{\text{s}}.500792(2)$, Dec = $19^\circ46'24''.22891(7)$ by the VLBA at 15.2 GHz (Atri et al. 2022).

Detections with several high-energy instruments have also been reported, including GeV emission with *Fermi*/LAT (potentially up to 400 GeV; Xia et al. 2024), TeV emission extending to 18 TeV from LHAASO (LHAASO Collaboration 2023), and even a suggestion of a possible association with a 250 TeV photon (Dzhappuev et al. 2022).

2.2. X-shooter spectroscopy

Following the detection of GRB 221009A, and motivated by the significant ambiguity in its distance (Galactic versus extragalactic), we initiated observations with the European Southern Observatory Very Large Telescope (ESO VLT Unit 3, Melipal)

located on Cerro Paranal (Chile) and the X-shooter spectrograph (Vernet et al. 2011). These observations began on 2022 October 10 at 00:49:26 UT (11.54 hr after the *Fermi* trigger). The source brightness at this time, as measured in our acquisition image, was $r' = 17.42 \pm 0.05$ mag (AB, calibrated against nearby stars from the Pan-STARRS catalog). A summary of the X-shooter spectroscopic observations is presented in Table 1.

Because of the limited target visibility, the airmass at the time of the observation was sizeable, but within the working range of the X-shooter atmospheric dispersion corrector (ADC). Observations were executed using the ABBA nod-on-slit mode, with a nod throw of about $6''$ along the slit. Each single arm spectrum was reduced in “stare” mode and using the standard X-shooter pipeline (Goldoni et al. 2006; Modigliani et al. 2010), with the extraction window at the position of the GRB afterglow trace, and background windows at both sides of the spectral trace. Then, for each exposure, residual sky features were interpolated using the background as reference (Selsing et al. 2019). Flux calibration was performed in two steps, first by applying the response function determined via observations of spectrophotometric standard stars, and then renormalizing the flux-calibrated spectra to the available photometry using the g , i , and H bands for the UVB, VIS, and NIR arms, respectively, interpolated at the mean time of the spectrum. Magnitudes were computed from images secured with the X-shooter acquisition camera or taken from a broader photometric set (Brivio et al. 2022; de Ugarte Postigo et al., in prep.). Finally, we applied a telluric correction built using a line-by-line radiative transfer model (LBLRTM; Clough et al. 1992) and the atmospheric properties, such as humidity, temperature, pressure, and zenith angle, which are stored in the header of each exposure.

The observations reveal a very bright trace in the red and infrared that is strongly attenuated toward the blue end by the high Galactic extinction. Figure 1 shows the overall shape of the spectrum and the inner panels zoom in on selected features. We subsequently obtained further X-shooter observations to follow the afterglow evolution. These are discussed in detail by de Ugarte Postigo et al. (in prep.). Among the late spectra, here we only present the 8×480 s spectrum, which has a mid time of 2022 October 20 00:20:01 UT and provides the best detection of the emission features (Fig. 1 and Sect. 3.3).

The results reported in this paper supersede our preliminary analysis (de Ugarte Postigo et al. 2022; Izzo et al. 2022). Our spectroscopic measurement was subsequently confirmed by Castro-Tirado et al. (2022).

3. Results

3.1. Absorption line system and redshift

In addition to several Galactic absorption features at $z = 0$, we identify a series of absorption lines including Ca II (4530, 4570 Å), Ca I (4867 Å), and Na I (6782, 6789 Å) at redshift

¹ Assuming a flat Λ CDM cosmology with $H_0 = 67.4 \text{ km s}^{-1} \text{ Mpc}^{-1}$ and $\Omega_m = 0.315$ (Planck Collaboration VI 2020).

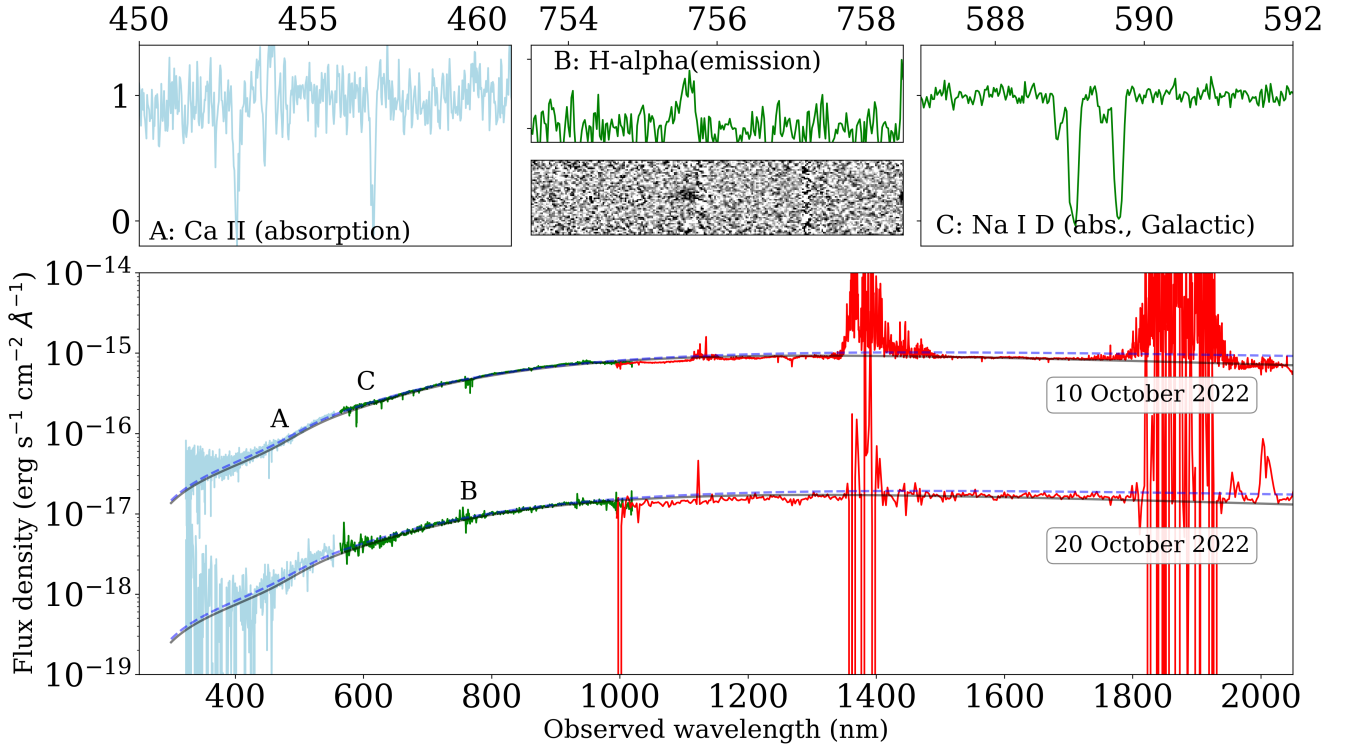


Fig. 1. Our X-shooter spectra of the afterglow of GRB 221009A on 2022 October 10 and 20. For clarity, the spectra shown in the bottom panel have been rebinned by a factor of 10 (first epoch) and 40 (second epoch). The UVB, VIS, and NIR arms are color coded in cyan, green, and red, respectively. The blue dashed lines show a power law with a spectral index of $\beta = 0.8$ ($F_\nu \propto \nu^{-\beta}$), extinguished by a foreground extinction of $A_V = 4.177$ mag, assuming the MW extinction law from Cardelli et al. (1989). The solid black lines show a bluer $\beta = 0.4$ spectrum with $A_V = 4.7$ mag, and provide a slightly better description of the data. The upper panels show zoomed-in regions around the Ca II absorption and H α emission at $z = 0.151$ (the afterglow continuum was digitally subtracted from the 2D plot) as well as the Na I D absorption complex due to dust in the MW.

$z \approx 0.151$. Unfortunately, at this low redshift, most of the strong metal lines are too far into the UV to be detected from the ground, and so we cannot carry out any in-depth analysis of the GRB host ISM.

We first analyzed the absorption features imprinted from the host-galaxy ISM on the afterglow spectrum. To this end, we used the Python package VoigtFit (Krogager 2018). This code creates a convolved spectrum based on the observed spectral resolution of the X-shooter spectra and simultaneously fits for the redshift z_{GRB} , broadening parameter b , and column density of each line complex. We tie the redshift to be identical across the five detected transitions in the optical (see Table 2). The best-fit redshift is $z_{\text{GRB}} = 0.15095 \pm 0.00005$. We also find that a single broadening parameter $b = 18.5 \pm 5.0$ km s $^{-1}$ is able to reproduce the observed line profiles (see Fig. 2), with total column densities of $\log(N_{\text{CaII}}/\text{cm}^{-2}) > 15.5$, $\log(N_{\text{CaI}}/\text{cm}^{-2}) = 12.19 \pm 0.08$, and $\log(N_{\text{NaI}}/\text{cm}^{-2}) = 12.21 \pm 0.01$. We note that the Ca II transitions are both saturated, and so the inferred column densities are quoted as 3σ lower limits.

We further note the presence of a well-detected absorption feature in the NIR arm observed at 12 468 Å, which we cannot associate with any telluric or Galactic transition. However, it matches the He I* 10 830 Å (unresolved) triplet at $z = 0.151$. The line profile reveals that the redshift and Doppler broadening of this particular feature are not consistent with the main ones described above, likely suggesting a different physical origin. From the best-fit Voigt profile, we find $z_{\text{HeI}^*} = 0.15089 \pm 0.00003$, $b = 40.9 \pm 1.3$ km s $^{-1}$, and a column density with $\log(N_{\text{HeI}^*}/\text{cm}^{-2}) = 12.29 \pm 0.01$. This feature was also identified by Fynbo et al. (2014) in the peculiar afterglow of

Table 2. Host absorption lines identified in the first X-shooter spectrum, with their measured equivalent widths (observer frame) and column densities.

Observed λ (Å)	Feature	EW (Å)	$\log(N/\text{cm}^{-2})$
4530.09	Ca II 3934.78	1.58 ± 0.1	> 15.5
4570.44	Ca II 3969.59	1.35 ± 0.09	> 15.5
4867.40	Ca I 4227.92	0.36 ± 0.06	12.19 ± 0.08
6782.87	Na I 5891.58	0.29 ± 0.01	12.21 ± 0.01
6789.71	Na I 5897.56	0.15 ± 0.01	12.21 ± 0.01
12 470.76	He I* 10830	1.025 ± 0.015	12.29 ± 0.01 ^(a)

Notes. ^(a) Best-fit column density with $z_{\text{HeI}^*} = 0.15089 \pm 0.00003$ and $b = 40.9 \pm 1.3$ km s $^{-1}$.

GRB 150406A at $z = 0.889$, and is also visible in the absorption spectrum of GRB 190114C at $z = 0.425$ (de Ugarte Postigo et al. 2020).

3.2. Extinction

The line of sight to GRB 221009A goes through significant foreground extinction from dust in the MW and potentially also within its host galaxy. The large foreground extinction is highlighted by strong absorption features seen at $z = 0$, such as K I and the strongly saturated Na I D (Fig. 1). In Fig. 1, we overplot the X-shooter spectra with a single power law with index $\beta = 0.8$ ($F_\nu \propto \nu^{-\beta}$; the same as observed in the X-ray after-

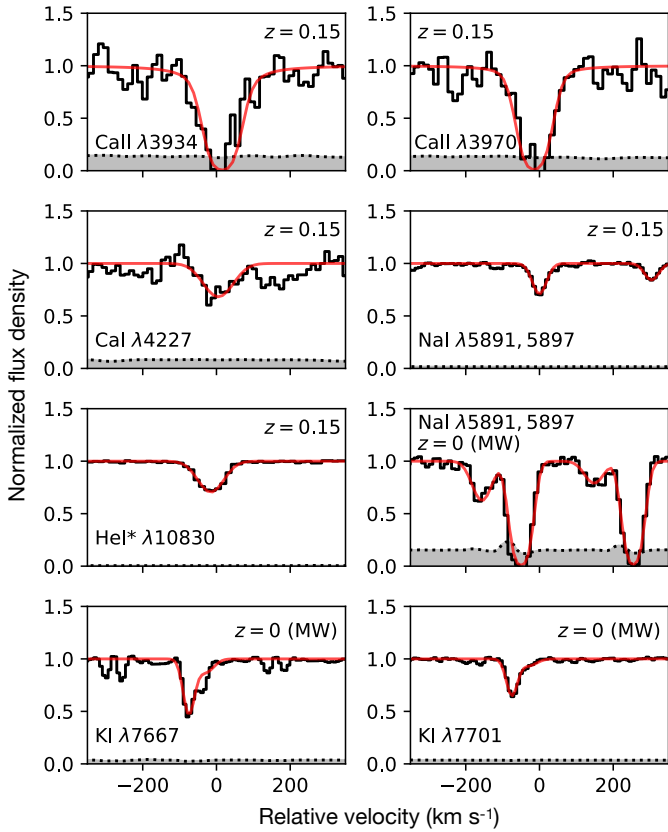


Fig. 2. Zoomed-in view of selected absorption features in velocity space. The gray-shaded areas show the error spectrum, while the red lines indicate the best-fit model. The KI 7667 Å line is affected by telluric absorption and was not used for the column density determination.

glow, e.g., Williams et al. 2023) with a foreground extinction of $A_V = 4.177$ mag (Schlafly & Finkbeiner 2011). This provides a reasonable description of the observations, but substantially over-predicts the measured flux in the red. This suggests the presence of additional extinction, either in the MW (a small underestimate, particularly toward the plane of the MW, is not unlikely) or due to additional dust inside the host galaxy. Given the low redshift of the event and the diversity of the extinction laws (Pei 1992), disentangling host from foreground extinction is nontrivial, but the overall results are relatively insensitive to the dust location. A better match to the data can be obtained with a larger total A_V . However, in this case the intrinsic spectral slope must be substantially bluer, matching the preferred results of Kann et al. (2023) and Levan et al. (2023) well. A Monte Carlo Markov Chain sampling of the data using a single power-law source with extinction described by a Fitzpatrick (1999) extinction law returns $A_V = 4.9$ mag and $R_V = 3.225$, with negligible host-galaxy extinction, and a power law with a spectral index of $\beta = 0.21$. This would be consistent with the presence of a cooling break lying between the X-ray and optical/IR band.

We also note that there is a significant revision in the foreground extinction between the map of Schlegel et al. (1998) and the recalibration of Schlafly & Finkbeiner (2011), which we have adopted, with the former value of $A_V = 4.8$ mag overall being consistent with our higher extinction scenario. Further insight into the dust location can be provided by the detection of Na I D at $z = 0.151$, which is often considered a dust tracer. Following Poznanski et al. (2012) and using the EWs from Table 2, we derive $A_V = 0.14^{+0.15}_{-0.11}$ mag, suggesting that indeed a (modest)

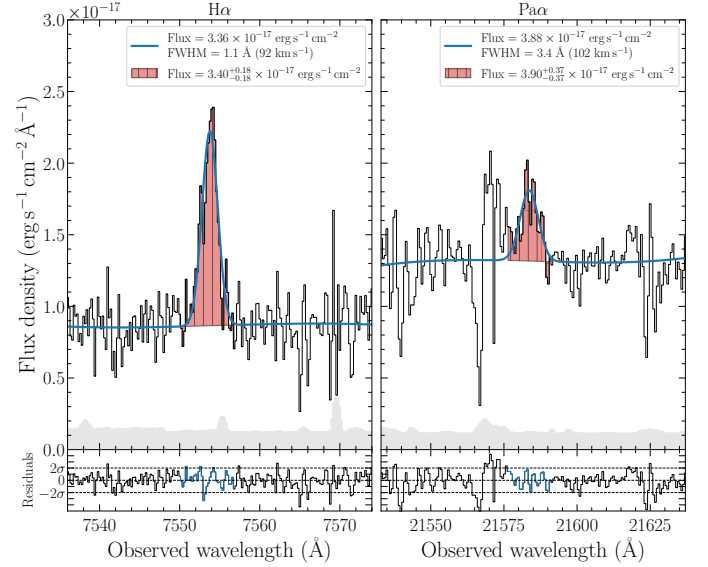


Fig. 3. Single-Gaussian fit to the $H\alpha$ (left) and $Pa\alpha$ (right) emission lines. A sky line is responsible for the large residuals blueward of $Pa\alpha$. Top panel: blue line is the result of the fit of the line and the continuum whose fit parameters are reported in the legend (the FWHM is measured in the observer frame). The red shaded area represents the direct integration of the observed flux, whose value is reported in the legend; this is the value used in the calculations throughout the paper. The gray shaded area represents the error spectrum. Bottom panel: normalised residuals. The blue points represent the region where the line is fit.

amount of dust is present in the GRB host galaxy along its line of sight, but that extra dust is also present in the MW, in excess of the Schlafly & Finkbeiner (2011) estimate.

3.3. Host galaxy

In addition to absorption lines, our X-shooter spectroscopy shows two emission lines from the underlying host galaxy. We detect $H\alpha$ (in the visible) and $Pa\alpha$ (in the NIR), while we cannot satisfactorily recover the bluer O III] $\lambda 5007$, O III] $\lambda 4959$, $H\beta$, or [O II] $\lambda\lambda 3726, 3729$, presumably due to the higher foreground extinction. A small spatial offset is observed between the afterglow trace and the $H\alpha$ emission line, which is consistent with the extension seen in Hubble Space Telescope imaging of the field (Levan et al. 2022, 2023; Fulton et al. 2023; Shrestha et al. 2023; see also Blanchard et al. 2024). This also implies that the measured fluxes are lower limits, as there is likely emission from regions not covered by the instrument slit. The slit was 0.9'' (1.1'') wide in the optical (NIR), and was oriented along the N-S direction, only partially covering the extended host galaxy. Line-flux ratios are however robust against slit losses. The flux of the detected lines was determined by fitting the continuum around each line and integrating the continuum-subtracted flux over the region of the line. We additionally fitted each detected line with a Gaussian profile, checking the consistency between the two values. The fits are shown in Fig. 3. We also computed an upper limit for [N II] $\lambda 6584$ as the flux of a Gaussian line with the same velocity width as $H\alpha$ and an amplitude equal to the noise estimated over the region where the line should lie.

The fluxes were then corrected for Galactic dust extinction using $A_V = 4.177$ mag and the MW extinction curve of Pei (1992). We determined the host galaxy A_V comparing the observed and theoretical ratio of the $H\alpha$ and $Pa\alpha$ lines

Table 3. Fluxes of the host emission lines measured in the X-shooter spectrum from October 20.

Line	Observed wavelength (Å)	Observed flux (10^{-17} erg s $^{-1}$ cm $^{-2}$)	Corrected flux (MW) (10^{-17} erg s $^{-1}$ cm $^{-2}$)	Corrected flux (MW + host) (10^{-17} erg s $^{-1}$ cm $^{-2}$)
H α	7553.80	$3.4^{+0.2}_{-0.2}$	$39.0^{+2.0}_{-2.0}$	$51.0^{+5.7}_{-5.6}$
P α	21 582.75	$3.9^{+0.4}_{-0.4}$	$5.7^{+0.5}_{-0.5}$	$6.0^{+0.7}_{-0.7}$
[N II] λ 6584	–	<0.4	<4.0	<5.3

Notes. The last two columns report the line fluxes corrected for the MW extinction ($A_V = 4.177$ mag) and MW + host, respectively.

($F(\text{H}\alpha)/F(\text{P}\alpha) = 8.56$) in the case B recombination scenario, with an electron temperature of 10 000 K and a density of 10^4 cm $^{-3}$ (Osterbrock & Ferland 2006). This method yields $A_V^{\text{host}} = 0.4^{+0.2}_{-0.2}$ mag, where the uncertainties are computed with Monte Carlo error propagation. As with the afterglow SED, it is not possible to disentangle whether this extra extinction is due to dust in the MW or in the GRB host, but this has little effect on our estimate given the low redshift of the object. All the fluxes and their corrected values are shown in Table 3.

Using the dust-corrected H α flux and the relation of Kennicutt (1998), we infer a star-formation rate (SFR) of $\text{SFR} = 0.16^{+0.02}_{-0.02} M_{\odot} \text{yr}^{-1}$, scaled to the initial mass function of Chabrier (2003), setting $z = 0.1510$ and a standard Planck Collaboration VI (2020) cosmology. Due to slit losses, this value should be considered as a lower limit.

Using the upper limit on the [N II] λ 6584 line, we can infer an upper limit on the metallicity of the host galaxy using the strong line calibrations of Maiolino et al. (2008), and taking $12 + \log(\text{O}/\text{H})_{\odot} = 8.69$ (Asplund et al. 2009). We find $12 + \log(\text{O}/\text{H}) < 8.5$ which is subsolar and is comparable to the typical metallicities found using the same method in long GRB hosts (Krühler et al. 2015; Japelj et al. 2016; Palmerio et al. 2019).

4. Discussion

4.1. Robustness of redshift

Given the challenges of explaining VHE emission from $z = 0.151$, it is relevant to consider whether or not there are other, lower redshift possibilities able to explain the burst. The presence of narrow absorption lines implies that the light from the GRB is passing through cool, low-velocity gas moving at a recessional velocity of $\sim 45\,000$ km s $^{-1}$. This is well beyond any plausible peculiar velocities for more local galaxies, or possible velocities of individual gas clouds within them. Although outflows (e.g., from SNe) can achieve high velocities, most do not reach $45\,000$ km s $^{-1}$, and in this case we would then expect to observe broad lines. Furthermore, the presence of narrow emission lines at $z = 0.151$ demonstrates that a star-forming galaxy at this redshift underlies the GRB position. The detection of a SN akin to SN 1998bw (Blanchard et al. 2024) further confirms the redshift value reported in this work.

We estimate the chance alignment probability P_{chance} between the afterglow and the galaxy using the formula presented by Bloom et al. (2002). Using HST imaging, Levan et al. (2023) report a $0.25''$ angular separation between the host centroid and the afterglow, and a host effective radius of $\approx 1''$. In this case, it is the latter quantity that should be used to compute P_{chance} . Using the host magnitude F625W = 24.88 AB, and correcting for the foreground extinction, we find $P_{\text{chance}} = 1 - 1.5 \times 10^{-3}$, where the uncertainty comes from the unknown proportion of extinction within the MW. Independent of this, the

chance alignment is very small, further solidifying the association with the galaxy and confirming the robustness of the GRB redshift identification.

Formally, we note that the detection of narrow absorption lines only places a lower limit on the burst redshift of $z = 0.151$. The redshift is such that we cannot detect individual variable fine-structure lines pumped by the UV emission from the GRB (e.g., Vreeswijk et al. 2004). It is plausible that the burst could be at even higher redshift. A higher redshift would ameliorate rate constraints, and could even be lensed by the $z = 0.151$ system (although such a scenario is very unlikely). However, placing the burst at an even higher redshift would only exacerbate the challenges of VHE emission and extreme prompt isotropic energy release. The lack of any detected features at redshifts of higher than $z = 0.151$ (including across wavelength ranges with high S/N) also argues against $z > 0.151$.

4.2. Energetics and implications

GRB 221009A is by far the brightest GRB ever observed (Burns et al. 2023c). Measurements of both the peak flux and fluence are underestimated because it was sufficiently bright to saturate many of the detectors, but even allowing for this, GRB 221009A was a factor of 40 more fluent than the next-brightest well-studied burst at the time², GRB 130427A (Ackermann et al. 2014; Preece et al. 2014; Maselli et al. 2014).

Estimating the precise isotropic energy release of GRB 221009A is nontrivial because of the difficulty in correcting for saturation effects. However, estimates of the fluence lie in the range $\approx (1-9) \times 10^{-2}$ erg cm $^{-2}$ (Gotz et al. 2022; Lesage et al. 2022; Frederiks et al. 2022; Kann & Agui Fernandez 2022) and the burst isotropic energy release in the 0.1 keV–100 MeV “ultrabroadband” band (Agüí Fernández et al. 2023) is at least $E_{\text{iso}} = 5.9 \times 10^{54}$ erg (Kann & Agui Fernandez 2022). In addition to being one of the closest, this makes GRB 221009A one of the most intrinsically energetic GRBs ever observed. If a more detailed saturation correction analysis yields a true fluence of $\gtrsim 10^{-1}$ erg cm $^{-2}$, GRB 221009A could well also be the most energetic GRB ever observed, at least within the sample of GRBs with known redshift.

4.3. Rates

The combination of proximity and brightness or energy release raises the question of just how unusual GRB 221009A is. To place this GRB in context, we compared it with long GRB events (i.e., those with $T_{90} > 2$ s) previously observed by Fermi/GBM. In general, it is relevant to consider both the peak flux and

² During the review process of this paper, another very bright event was observed, which has now become the second brightest detected GRB; (Burns et al. 2023a).

the fluence. While the peak flux is normally more relevant for triggering, in the case of GRB 221009A it is also likely more difficult to correct for saturation compared to fluence. We thus considered both the “bolometric” 1–10 000 keV band fluence³ and the peak count rates, calculated with 1024 ms binning, summed over all NaI detectors and all channels. To construct the latter, we downloaded all `trigdata` files related to long GRBs from the *Fermi*/GBM trigger catalog⁴ and used the count-rate data therein. In 98% of cases, peak count rates were reported with a binning of 1024 ms or finer (in which case we downsampled to 1024 ms by summing neighboring bins near the peak). We assumed the remaining 2% of the events to be sampled from the same distribution. From these, we constructed the corresponding inverse cumulative distributions, which are shown in Fig. 4. In order to convert the number of observed events into an all-sky rate, we divided the number by the GBM mission duration ($T_{\text{GBM}} = 10$ yr, as we used only bursts whose spectral information is part of the fourth *Fermi*/GBM catalog; von Kienlin et al. 2020), and by the effective GBM duty cycle $\eta = 0.598$, determined by its limited field of view and downtime, itself attributable to the need to turn off the detectors during the transit through the South Atlantic anomaly (Burns et al. 2016). In order to extrapolate the observed inverse cumulative distribution to the fluence (or count rate) of GRB 221009A, we identified a fluence (or count rate) f_0 above which the distribution resembles a single power law and fitted a simple power-law model with index a to the data above that point (excluding GRB 221009A itself). The fit is performed in a Bayesian fashion, as follows. The assumed probability of observing a given fluence (or count rate) f_i is $p(f_i | a) = (a/f_0)(f_i/f_0)^{-a-1}$, and therefore the posterior probability on a given the observed fluences (or count rates) is

$$p(a | \mathbf{d}) \propto \pi(a) \prod_{i=1}^{N_0} \frac{a}{f_0} \left(\frac{f_i}{f_0} \right)^{-a-1}, \quad (1)$$

where $\mathbf{d} = \{f_i\}_{i=1}^{N_0}$ is our data and $\pi(a)$ is the prior on a , which we take as uniform in a , $\pi(a) \propto 1$. We set $f_0 = 10^{-4}$ erg cm⁻² for fluences and $f_0 = 10^4$ ct s⁻¹ for count rates. The posterior probability density distributions on a are nearly Gaussian for both the fluence and count rate cases, and yield $a \sim 1.66^{+0.31}_{-0.28}$ for fluences and $a \sim 1.52 \pm 0.13$ for count rates (median and symmetric 68% credible interval). While the slope in both cases is close to $a = 3/2$, which is expected for homogeneously distributed sources in Euclidean space, this is not, in this case, indicating such a distribution, but is caused by the increase in the GRB rate with redshift ($\propto (1+z)^{3.2}$; Ghirlanda & Salvaterra 2022), which, in this calculation, cancels out the effect of the expansion of the Universe. Given the power-law scaling, the expected all-sky rate of events above a fluence (or count rate) f^* is simply

$$\bar{R}_{\text{obs}}(f \geq f^*) = \frac{N_0}{T_{\text{GBM}}\eta} \left(\frac{f^*}{f_0} \right)^{-a}. \quad (2)$$

³ We used the information available in the online *Fermi*/GBM catalog, accessible at <https://heasarc.gsfc.nasa.gov/W3Browse/fermi/fermigbrst.html>, focusing on bursts detected up to November 26 2018, which were published in the fourth *Fermi*/GBM catalog (von Kienlin et al. 2020). For bursts with available spectral information, we used the best-fitting spectral model (as reported in the `flnc_best_fitting_model` column) with the reported best-fit parameters to compute the bolometric fluence. For the remaining $\sim 5.8\%$ of the bursts, we used the 10–1000 keV value reported in the `fluence` column, which is a good approximation of the bolometric fluence, assuming the peak of the νF_ν spectrum is below 1000 keV.

⁴ <https://heasarc.gsfc.nasa.gov/W3Browse/fermi/fermigtrig.html>

Figure 4 shows the resulting expected rate extrapolation, which is compared to the GRB 221009A bolometric fluence $f^* \sim 0.2$ erg cm⁻² (Frederiks et al. 2023; Burns et al. 2023c) and to its peak count rate of $f^* = 1.7 \times 10^6$ ct s⁻¹ obtained as explained above. The latter is a lower limit because of the saturation in the NaI detectors.

Taking the values corresponding to the 90th percentiles of the posterior distributions, we estimate a rate of less than 1 event in 4210 years (fluences) or 70 years (peak count rate) as bright as or brighter than GRB 221009A. The former value is much lower than that found by Atteia (2022), owing to the fact that we employ a bolometric, saturation-corrected estimate of the brightness of this burst.

Given these expected rates, the probability of observing at least one event with *Fermi*/GBM, assuming Poisson statistics, is given by

$$p(N(f \geq f^*) > 0 | \mathbf{d}) = 1 - p(N(f \geq f^*) = 0 | \mathbf{d}) \\ = 1 - \int \exp(-\bar{R}_{\text{obs}}\eta T_{\text{GBM}}) p(a | \mathbf{d}) da, \quad (3)$$

which yields $p(N(f \geq f^*) > 0 | \mathbf{d}) \sim 6.8 \times 10^{-4}$ using the fluences, and $p(N(f \geq f^*) > 0 | \mathbf{d}) \lesssim 0.064$ using the count rates. Again, the latter must be taken as an upper limit due to saturation. These values confirm that GRB 221009A is a very rare event, in agreement with Burns et al. (2023c).

4.4. Estimate based on a GRB population model

We also provide an estimate of the rate of GRB 221009A-like events based on the state-of-the-art model for the population of long GRBs described in Ghirlanda & Salvaterra (2022). This model predicts the intrinsic properties of the population of long GRBs, such as their luminosity function and cosmic rate, as obtained by reproducing the observed distributions of the properties of bursts detected by *Fermi*/GBM and CGRO/BATSE, and the distributions of rest-frame properties of a flux-limited sample of bright GRBs detected by *Swift*/BAT (Salvaterra et al. 2012). By sampling the posterior distribution of the model population parameters (Table 1 in Ghirlanda & Salvaterra 2022), we estimated the probability of occurrence of an event with an isotropic-equivalent luminosity $L \geq L_*$ within a redshift of $z \leq z_*$, where $L_* = 10^{54}$ erg s⁻¹ (Burns et al. 2023c) and $z_* = 0.15$ correspond to the values of GRB 221009A. With these values, we sampled the population model posterior probability and derived a mean rate of 1 every 18 400 yr (or 1 every 3150 yr as 90th percentile estimate).

In the entirety of 55 years of GRB observations, no event has been reported that even comes close to GRB 221009A in terms of fluence (Burns et al. 2023c). Prior to GRB 221009A, GRB 130427A was very likely the most fluent GRB of the combined CGRO/BATSE, Konus/*Wind*, and *Fermi*/GBM era beginning in 1991, which is well documented and readily publicly available (Paciesas et al. 1999; Kaneko et al. 2006; Nava et al. 2011; Goldstein et al. 2013; Tsvetkova et al. 2017, 2021; Ajello et al. 2019; von Kienlin et al. 2020). More recently, *Fermi* detected another high-fluence event, namely GRB 230307A with a preliminary estimate of the fluence of $\sim 3 \times 10^{-3}$ erg cm⁻² (Dalessi & Fermi GBM Team 2023), comparable to that of GRB 130427A and also a very rare (once per few decades) event (Burns et al. 2023b; Levan et al. 2024).

The situation for the first ~ 25 years of GRB studies is less transparent, but there are several events with fluences similar to that of GRB 130427A, namely the famous GRB 830801B

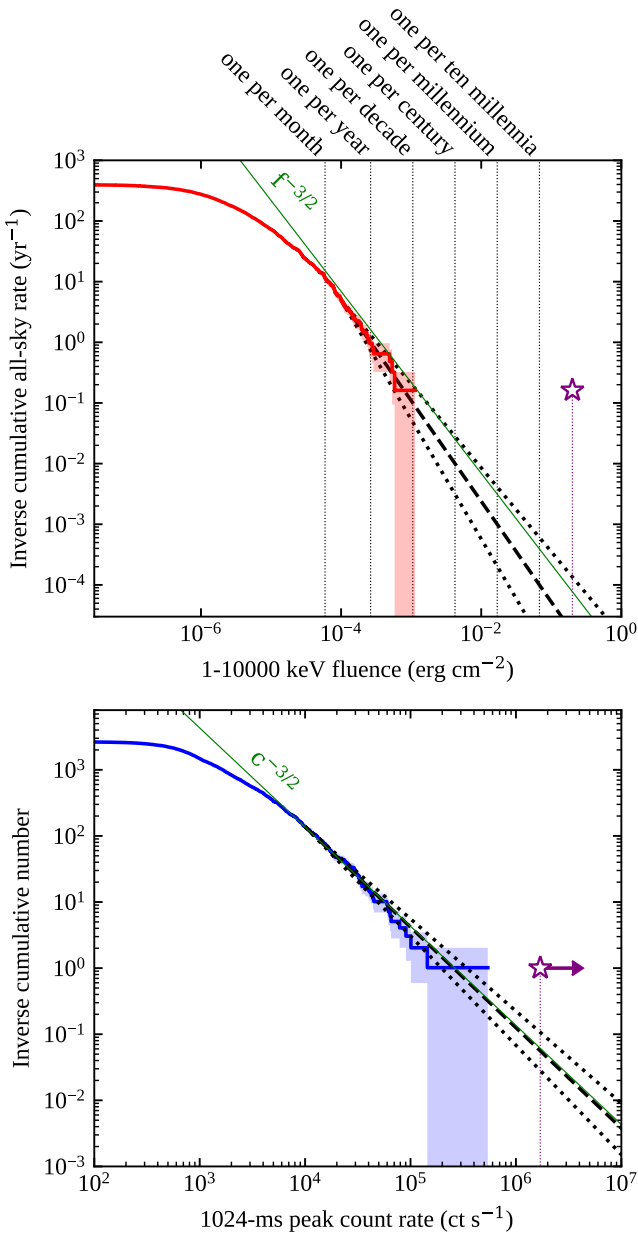


Fig. 4. Differential and integrated GRB rates. Top panel: all-sky cumulative rate of long GRBs (i.e., those with $T_{90} > 2$ s; thick solid line) observed by *Fermi*/GBM up to 2018 June above a given 1–10 000 keV fluence, excluding GRB 221009A. The estimated fluence of the latter, ~ 0.2 erg cm $^{-2}$, based on *Fermi*/GBM (Lesage et al. 2022; Burns et al. 2023c), *Konus/Wind* (Frederiks et al. 2023), *INSIGHT-HXMT*, and *GECAM-C* (An et al. 2023), is shown by the purple star. The shaded area comprises the distributions obtained by varying the observed number by \sqrt{N} , where N is the number of bursts in each bin, which approximates the Poisson error. The black dashed line shows the best-fit power-law model $N(> f) = N_0(f/f_0)^{-a}$, where $f_0 = 10^{-4}$ erg cm $^{-2}$ and N_0 is the observed rate above f_0 . The black dotted lines encompass the 68% uncertainty on the power-law index a from such a fit. The thin green line shows the theoretically expected $-3/2$ scaling for homogeneously distributed sources in Euclidean space although there is no strong expectation that GRBs should follow this distribution (see text). The vertical dotted lines mark the fluxes that correspond to the reported rates according to the best-fit power-law model. Bottom panel: similar to the top panel, but showing the cumulative number of events above a given peak background-subtracted count rate (summed over all channels and all NaI detectors, measured with 1024 ms binning, and not corrected for saturation). In this case, $f_0 = 10^4$ ct s $^{-1}$, and the peak count rate of GRB 221009A is a lower limit.

(Kuznetsov et al. 1986, 1987; Schaefer et al. 2001), the significantly less well-documented GRB 840304 (Klebesadel et al. 1984; Itoh et al. 1985), and two events detected by the Pioneer Venus Orbiter (PVO), GRBs 920212 and 900808 (the latter mentioned in Fenimore et al. 1996 as the brightest GRB in terms of peak flux detected by PVO). However, none of these events had a fluence in excess of 10^{-2} erg cm $^{-2}$, and so GRB 221009A is potentially more than ten times as fluent as any other GRB ever detected (Burns et al. 2023c).

4.5. VHE emission

One of the most striking features of the detection of GRB 221009A is the identification of very high-energy emission. In particular, the LHAASO water Cherenkov observatory reported the detection of more than 5000 TeV photons associated with the burst (Huang et al. 2022; LHAASO Collaboration 2023; Cao et al. 2023), with a highest energy photon at 18 TeV. The Carpet-2 experiment detected a possible 250 TeV photon (Dzhappuev et al. 2022).

Knowledge of the redshift is critical for the interpretation of these observations, because TeV photons scatter off the extragalactic background light (EBL) photons or even – at the very highest energies – off the cosmic microwave background (CMB) photons. The EBL is the result of photons from essentially every photon emitter in the Universe, and is therefore, in addition to the CMB, of important cosmological utility. These photon scatterings result in progressively higher opacity for photons of increasing energy. The detection of high-energy TeV photons is therefore a valuable route to probing models for the EBL.

Indeed, the detection of such emission from GRB 221009A at $z = 0.151$ is particularly intriguing. For example, by reconstructing the expected intrinsic emission from blazars, Domínguez et al. (2013) estimated the effective horizon as a function of photon energy: at 18 TeV this horizon (corresponding to an optical depth of 1, or an attenuation factor of 0.63) lies at $z < 0.01$, while at $z = 0.15$, $\tau \gg 3$ (attenuation > 0.95). In practice, the situation is less severe, because the uncertainty associated with the highest-energy photons is significant (formally Cao et al. 2023 find $E = 17.8^{+7.4}_{-5.1}$ TeV) and because alternative, nonphotonic (e.g., muon) origins cannot be robustly ruled out. However, there remains some tension that may be suggestive of either lower-than-expected opacity in the EBL or new physics (Cao et al. 2023; Galanti et al. 2023).

Knowledge of the redshift also provides robust constraints on the total neutrino luminosity for the GRB. Intensive study of candidate neutrino tracks in the IceCube experiment provided no evidence for any neutrino excess in the MeV, TeV, and PeV energy ranges Abbasi et al. (2023). Indeed, because of the proximity and high-energy emission (the processes for which can also create neutrinos), constraints on neutrino production for GRB 221009A are as strong as those from stacked analyses of larger numbers of bursts (Murase et al. 2022), and begin to provide meaningful constraints on at least some physical parameters within the fireball (e.g., bulk Lorentz factor and dissipation radius; see Murase et al. 2022; Abbasi et al. 2023).

5. Conclusions

We present a measurement of the redshift of GRB 221009A with the VLT/X-shooter. Our observations allow us to measure $z = z_{\text{GRB}} = 0.15095 \pm 0.00005$, demonstrating that GRB 221009A is not only the brightest GRB ever seen (in terms of flux and fluence) but is also intrinsically one of the most energetic.

From the fluxes of a few emission lines detected on top of the afterglow spectrum, we are also able to constrain the SFR, metallicity, and dust content of the host galaxy. The values found are consistent with those of GRB host galaxies at low redshift.

In addition to the large tabulated amount of extinction in the direction of the GRB due to the MW ($A_V = 4.177$ mag), we detect extra absorption (by ≈ 0.5 mag). From the shape of the afterglow SED, the fluxes of the host emission lines, and the detection of Na I in absorption, we suggest that about 0.15 mag of extinction is located in the GRB host, with the remaining lying in the MW.

Our analysis suggests that a burst this close and this luminous should only be witnessed at best once every few decades, and may be as rare as a once-per-millennium event, depending on its actual flux and fluence values.

Acknowledgements. We dedicate this paper to the memory of our beloved colleagues David Alexander “Alex” Kann, who was especially fond of this unique GRB. We are grateful for a constructive report from an anonymous referee. This paper is based on observations collected at the European Southern Observatory under ESO programme 110.24CF (PI Tanvir). We thank the support from the ESO observing staff in Paranal, in particular Cédric Ledoux, Matias Jones, Michael Abdul-Masih, Zahed Wahhaj. PDA acknowledge funding from the Italian Space Agency, contract ASI/INAF n. I/004/11/4 and from PRIN-MIUR 2017 (grant 20179ZF5KS). DAK acknowledges the support by the State of Hessen within the Research Cluster ELEMENTS (Project ID 500/10.006). DBM, AJL and NRT are supported by the European Research Council (ERC) under the European Union’s Horizon 2020 research and innovation programme (grant agreement No. 725246). The Cosmic Dawn Center is supported by the Danish National Research Foundation. JH and LI were supported by a VIL-LUM FONDEN Investigator grant (project number 16599). EPI acknowledges financial support through an INAF research grant. MER acknowledges support from the research programme Athena with project number 184.034.002, which is financed by the Dutch Research Council (NWO). AS and SDV acknowledge support from DIM-ACAV+. KW acknowledges support through a UK Research and Innovation Future Leaders Fellowship awarded to Dr. B. Simmons (MR/T044136/1). DX acknowledges the science research grants from the China Manned Space Project with NO. CMS-CSST-2021-A13 and CMS-CSST-2021-B11.

References

- Abbasi, R., Ackermann, M., Adams, J., et al. 2023, *ApJ*, 946, L26
 Ackermann, M., Ajello, M., Asano, K., et al. 2014, *Science*, 343, 42
 Agüí Fernández, J. F., Thöne, C. C., Kann, D. A., et al. 2023, *MNRAS*, 520, 613
 Ajello, M., Arimoto, M., Axelsson, M., et al. 2019, *ApJ*, 878, 52
 An, Z. H., Antier, S., Bi, X. Z., et al. 2023, ArXiv e-prints [arXiv:2303.01203]
 Asplund, M., Grevesse, N., Sauval, A. J., & Scott, P. 2009, *ARA&A*, 47, 481
 Atri, P., An, T., Giroletti, M., et al. 2022, *GRB Coordinates Network*, 32907
 Atteia, J. L. 2022, *GRB Coordinates Network*, 32793
 Bissaldi, E., Omodei, N., Kerr, M., & Fermi-LAT Team 2022, *GRB Coordinates Network*, 32637
 Blanchard, P. K., Villar, V. A., Chornock, R., et al. 2024, *Nature Astronomy*, 8, 774
 Bloom, J. S., Kulkarni, S. R., & Djorgovski, S. G. 2002, *AJ*, 123, 1111
 Bloom, J. S., Perley, D. A., Li, W., et al. 2009, *ApJ*, 691, 723
 Brivio, R., Ferro, M., D’Avanzo, P., et al. 2022, *GRB Coordinates Network*, 32652
 Burns, E., Connaughton, V., Zhang, B.-B., et al. 2016, *ApJ*, 818, 110
 Burns, E., Goldstein, A., Lesage, S., & Dalessi, S. 2023a, *GRB Coordinates Network*, 33414, 1
 Burns, E., Goldstein, A., Lesage, S., Dalessi, S., & Fermi-GBM Team 2023b, *GRB Coordinates Network*, 33414, 1
 Burns, E., Svinkin, D., Fenimore, E., et al. 2023c, *ApJ*, 946, L31
 Cano, Z., Wang, S.-Q., Dai, Z.-G., & Wu, X.-F. 2017, *Advances in Astronomy*, 2017, 8929054
 Cao, Z., Aharonian, F., An, Q., et al. 2023, *Science Advances*, 9, ead7278
 Cardelli, J. A., Clayton, G. C., & Mathis, J. S. 1989, *ApJ*, 345, 245
 Castro-Tirado, A. J., Sanchez-Ramirez, R., Hu, Y. D., et al. 2022, *GRB Coordinates Network*, 32686
 Cenko, S. B., Frail, D. A., Harrison, F. A., et al. 2011, *ApJ*, 732, 29
 Chabrier, G. 2003, *PASP*, 115, 763
 Clough, S. A., Iacono, M. J., & Moncet, J.-L. 1992, *J. Geophys. Res.*, 97, 15761
 Cucchiara, A., Levan, A. J., Fox, D. B., et al. 2011, *ApJ*, 736, 7
 Dalessi, S., & Fermi GBM Team 2023, *GRB Coordinates Network*, 33407, 1
 de Ugarte Postigo, A., Thöne, C. C., Martín, S., et al. 2020, *A&A*, 633, A68
 de Ugarte Postigo, A., Izzo, L., Pugliese, G., et al. 2022, *GRB Coordinates Network*, 32648
 D’Elia, V., Pian, E., Melandri, A., et al. 2015, *A&A*, 577, A116
 Dichiarà, S., Gropp, J. D., Kennea, J. A., et al. 2022a, *The Astronomer’s Telegram*, 15650
 Dichiarà, S., Gropp, J. D., Kennea, J. A., et al. 2022b, *GRB Coordinates Network*, 32632
 Domínguez, A., Finke, J. D., Prada, F., et al. 2013, *ApJ*, 770, 77
 Dzhappuev, D. D., Afashokov, Y. Z., Dzaparova, I. M., et al. 2022, *The Astronomer’s Telegram*, 15669
 Fenimore, E. E., Klebesadel, R. W., & Laros, J. G. 1996, *ApJ*, 460, 964
 Fitzpatrick, E. L. 1999, *PASP*, 111, 63
 Franceschini, A., & Rodighiero, G. 2017, *A&A*, 603, A34
 Frederiks, D., Lysenko, A., Ridnaia, A., et al. 2022, *GRB Coordinates Network*, 32668
 Frederiks, D., Svinkin, D., Lysenko, A. L., et al. 2023, *ApJ*, 949, L7
 Frederiks, D. D., Hurley, K., Svinkin, D. S., et al. 2013, *ApJ*, 779, 151
 Fulton, M. D., Smartt, S. J., Rhodes, L., et al. 2023, *ApJ*, 946, L22
 Fynbo, J. P. U., Krühler, T., Leighly, K., et al. 2014, *A&A*, 572, A12
 Galama, T. J., Vreeswijk, P. M., van Paradijs, J., et al. 1998, *Nature*, 395, 670
 Galanti, G., Nava, L., Roncadelli, M., Tavecchio, F., & Bonnoli, G. 2023, *Phys. Rev. Lett.*, 131, 251001
 Ghirlanda, G., & Salvaterra, R. 2022, *ApJ*, 932, 10
 Gilmore, R. C., Somerville, R. S., Primack, J. R., & Domínguez, A. 2012, *MNRAS*, 422, 3189
 Goldoni, P., Royer, F., François, P., et al. 2006, in *SPIE Conf. Ser.*, eds. I. S. McLean, & M. Iye, 6269, 62692K
 Goldstein, A., Preece, R. D., Malozzi, R. S., et al. 2013, *ApJS*, 208, 21
 Gotz, D., Mereghetti, S., Savchenko, V., et al. 2022, *GRB Coordinates Network*, 32660
 Hjorth, J., & Bloom, J. S. 2012, *Chapter 9 in “Gamma-Ray Bursts*, 169
 Huang, Y., Hu, S., Chen, S., et al. 2022, *GRB Coordinates Network*, 32677
 Itoh, M., Fenimore, E. E., Fikani, M., et al. 1985, *Bulletin of the American Astronomical Society*, 17, 850
 Izzo, L., Saccardi, A., Fynbo, J. P. U., et al. 2022, *GRB Coordinates Network*, 32765
 Izzo, L., Thöne, C. C., Schulze, S., et al. 2017, *MNRAS*, 472, 4480
 Japelj, J., Vergani, S. D., Salvaterra, R., et al. 2016, *A&A*, 590, A129
 Kaneko, Y., Preece, R. D., Briggs, M. S., et al. 2006, *ApJS*, 166, 298
 Kann, D. A., Agayeva, S., Aivazyan, V., et al. 2023, *ApJ*, 948, L12
 Kann, D. A., & Agui Fernandez, J. F. 2022, *GRB Coordinates Network*, 32762
 Kann, D. A., Masetti, N., & Klose, S. 2007, *AJ*, 133, 1187
 Kennea, J. A., Williams, M., & Swift Team 2022, *GRB Coordinates Network*, 32635
 Kennicutt, R. C., Jr 1998, *ApJ*, 498, 541
 Klebesadel, R. W., Laros, J. G., & Fenimore, E. E. 1984, *Bulletin of the American Astronomical Society*, 16, 1016
 Krogager, J. K. 2018, ArXiv e-prints [arXiv:1803.01187]
 Krühler, T., Malesani, D., Fynbo, J. P. U., et al. 2015, *A&A*, 581, A125
 Krühler, T., Kuncarayakti, H., Schady, P., et al. 2017, *A&A*, 602, A85
 Kuznetsov, A. V., Syunyaev, R. A., Terekhov, O. V., et al. 1986, *Soviet Astronomy Letters*, 12, 315
 Kuznetsov, A. V., Sunyaev, R. A., Terekhov, O. V., et al. 1987, *Pisma v Astronomicheskii Zhurnal*, 13, 1055
 Lapshov, I., Molkov, S., Mereminsky, I., et al. 2022, *GRB Coordinates Network*, 32663
 Lesage, S., Veres, P., Briggs, M. S., et al. 2023, *ApJ*, 952, L42
 Lesage, S., Veres, P., Roberts, O. J., et al. 2022, *GRB Coordinates Network*, 32642
 Levan, A. J., Barclay, T., Bhirimbhakti, K., et al. 2022, *GRB Coordinates Network*, 32921
 Levan, A. J., Lamb, G. P., Schneider, B., et al. 2023, *ApJ*, 946, L28
 Levan, A. J., Gompertz, B. P., Salafia, O. S., et al. 2024, *Nature*, 626, 737
 LHAASO Collaboration (Cao, Z., et al.) 2023, *Science*, 380, 1390
 Lipunov, V., Kornilov, V., Gorbvskoy, E., et al. 2022, *GRB Coordinates Network*, 32634
 Liu, J. C., Zhang, Y. Q., Xiong, S. L., et al. 2022, *GRB Coordinates Network*, 32751
 Maiolino, R., Nagao, T., Grazian, A., et al. 2008, *A&A*, 488, 463
 Maselli, A., Melandri, A., Nava, L., et al. 2014, *Science*, 343, 48
 Mitchell, L. J., Philips, B. F., & Johnson, W. N. 2022, *GRB Coordinates Network*, 32746
 Modigliani, A., Goldoni, P., Royer, F., et al. 2010, in *Observatory Operations: Strategies, Processes, and Systems*, eds. D. R. Silva, A. B. Peck, & B. T. Soifer, *SPIE Conf. Ser.*, 7737, 773728

- Murase, K., Mukhopadhyay, M., Kheirandish, A., Kimura, S. S., & Fang, K. 2022, *ApJ*, **941**, L10
- Nava, L., Ghirlanda, G., Ghisellini, G., & Celotti, A. 2011, *A&A*, **530**, A21
- Osterbrock, D. E., & Ferland, G. J. 2006, *Astrophysics of Gaseous Nebulae and Active Galactic Nuclei* (Sausalito: University Science Books)
- Paciesas, W. S., Meegan, C. A., Pendleton, G. N., et al. 1999, *ApJS*, **122**, 465
- Palmerio, J. T., Vergani, S. D., Salvaterra, R., et al. 2019, *A&A*, **623**, A26
- Pei, Y. C. 1992, *ApJ*, **395**, 130
- Piano, G., Verrecchia, F., Bulgarelli, A., et al. 2022, *GRB Coordinates Network*, **32657**
- Planck Collaboration VI 2020, *A&A*, **641**, A6
- Poznanski, D., Prochaska, J. X., & Bloom, J. S. 2012, *MNRAS*, **426**, 1465
- Preece, R., Burgess, J. M., von Kienlin, A., et al. 2014, *Science*, **343**, 51
- Racusin, J. L., Karpov, S. V., Sokolowski, M., et al. 2008, *Nature*, **455**, 183
- Ripa, J., Pal, A., Werner, N., et al. 2022, *GRB Coordinates Network*, **32685**, 1
- Rodi, J., & Ubertini, P. 2023, *A&A*, **677**, L3
- Salvaterra, R., Della Valle, M., Campana, S., et al. 2009, *Nature*, **461**, 1258
- Salvaterra, R., Campana, S., Vergani, S. D., et al. 2012, *ApJ*, **749**, 68
- Schaefer, B. E., Deng, M., & Band, D. L. 2001, *ApJ*, **563**, L123
- Schlafly, E. F., & Finkbeiner, D. P. 2011, *ApJ*, **737**, 103
- Schlegel, D. J., Finkbeiner, D. P., & Davis, M. 1998, *ApJ*, **500**, 525
- Schulze, S., Malesani, D., Cucchiara, A., et al. 2014, *A&A*, **566**, A102
- Selsing, J., Malesani, D., Goldoni, P., et al. 2019, *A&A*, **623**, A92
- Shrestha, M., Sand, D. J., Alexander, K. D., et al. 2023, *ApJ*, **946**, L25
- Soderberg, A. M., Kulkarni, S. R., Berger, E., et al. 2004, *Nature*, **430**, 648
- Tan, W. J., Li, C. K., Ge, M. Y., et al. 2022, *The Astronomer's Telegram*, **15660**, 1
- Tanga, M., Krühler, T., Schady, P., et al. 2018, *A&A*, **615**, A136
- Tanvir, N. R., Fox, D. B., Levan, A. J., et al. 2009, *Nature*, **461**, 1254
- Tanvir, N. R., Laskar, T., Levan, A. J., et al. 2018, *ApJ*, **865**, 107
- Tavani, M., Piano, G., Bulgarelli, A., et al. 2023, *ApJ*, **956**, L23
- Tsvetkova, A., Frederiks, D., Golenetskii, S., et al. 2017, *ApJ*, **850**, 161
- Tsvetkova, A., Frederiks, D., Svinkin, D., et al. 2021, *ApJ*, **908**, 83
- Ursi, A., Panebianco, G., Pittori, C., et al. 2022, *GRB Coordinates Network*, **32650**
- Veres, P., Burns, E., Bissaldi, E., et al. 2022, *GRB Coordinates Network*, **32636**, 1
- Vernet, J., Dekker, H., D'Odorico, S., et al. 2011, *A&A*, **536**, A105
- von Kienlin, A., Meegan, C. A., Paciasas, W. S., et al. 2020, *ApJ*, **893**, 46
- Vreeswijk, P. M., Ellison, S. L., Ledoux, C., et al. 2004, *A&A*, **419**, 927
- Řípa, J., Takahashi, H., Fukazawa, Y., et al. 2023, *A&A*, **677**, L2
- Williams, M. A., Kennea, J. A., Dichiara, S., et al. 2023, *ApJ*, **946**, L24
- Xia, Z.-Q., Wang, Y., Yuan, Q., & Fan, Y.-Z. 2024, *Nature Communications*, **15**, 4280
- Xiao, H., Krucker, S., & Daniel, R. 2022, *GRB Coordinates Network*, **32661**
- ⁷ INAF, Osservatorio Astronomico di Brera, via E. Bianchi 46, I-23807 Merate (LC), Italy
- ⁸ INFN – Sezione di Milano-Bicocca, Piazza della Scienza 3, I-20146 Milano (MI), Italy
- ⁹ Hessian Research Cluster ELEMENTS, Giersch Science Center, Max-von-Laue-Strasse 12, Goethe University Frankfurt, Campus Riedberg, 60438 Frankfurt am Main, Germany
- ¹⁰ Astrophysics Research Institute, Liverpool John Moores University, 146 Brownlow Hill, Liverpool L3 5RF, UK
- ¹¹ GEPI, Observatoire de Paris, Université PSL, CNRS, 5 Place Jules Janssen, 92190 Meudon, France
- ¹² INAF, Istituto di Astrofisica Spaziale e Fisica cosmica, Via Alfonso Corti 12, I-20133 Milano (MI), Italy
- ¹³ School of Physics and Astronomy, University of Leicester, University Road, LE1 7RH Leicester, United Kingdom
- ¹⁴ Instituto de Astrofísica de Andalucía – CSIC, Glorieta de la Astronomía s/n, 18008 Granada, Spain
- ¹⁵ European Space Agency (ESA), European Space Research and Technology Centre (ESTEC), Keplerlaan 1, 2201 AZ Noordwijk, The Netherlands
- ¹⁶ ASI – Italian Space Agency, Space Science Data Centre, Via del Politecnico snc, 00133 Rome, Italy
- ¹⁷ INAF, Osservatorio Astronomico di Capodimonte, Salita Moiarriello 16, 80131 Napoli, Italy
- ¹⁸ Department of Mathematics, Informatics, Physics and Earth Sciences, University of Messina, Via F. D'Alcontres 31, Papardo, Messina 98166, Italy
- ¹⁹ School of Physics and Astronomy & Institute for Gravitational Wave Astronomy, University of Birmingham, Birmingham B15 2TT, United Kingdom
- ²⁰ Department of Physics and Astronomy, Kinard Lab of Physics, Clemson University, Clemson, SC 29634, USA
- ²¹ Centre for Astrophysics and Cosmology, Science Institute, University of Iceland, Dunhagi 5, 107 Reykjavík, Iceland
- ²² INAF–Osservatorio di Astrofisica e Scienza dello Spazio, Via Piero Gobetti 93/3, 40024 Bologna, Italy
- ²³ Astronomical Institute Anton Pannekoek, University of Amsterdam, 1090 GE Amsterdam, The Netherlands
- ²⁴ Department of Physics, University of Bath, Bath BA2 7AY, United Kingdom
- ²⁵ Kavli Institute for Astrophysics and Space Research, Massachusetts Institute of Technology, 77 Massachusetts Ave, Cambridge, MA 02139, USA
- ²⁶ The Oskar Klein Centre, Department of Astronomy, Stockholm University, AlbaNova SE-106 91 Stockholm, Sweden
- ²⁷ Astronomical Institute of the Czech Academy of Sciences, Fričova 298, 251 65 Ondřejov, Czech Republic
- ²⁸ Department of Physics, George Washington University, 725 21st St NW, Washington, DC 20052, USA
- ²⁹ Physics Department, Lancaster University, Lancaster LA1 4YB, United Kingdom
- ³⁰ Key Laboratory of Space Astronomy, National Astronomical Observatories, Chinese Academy of Sciences, Beijing 100101, China
- ³¹ School of Mathematical and Physical Sciences, Macquarie University, NSW 2109, Australia

¹ Department of Astrophysics/IMAPP, Radboud University, 6525 AJ Nijmegen, The Netherlands

² Cosmic Dawn Center (DAWN), Copenhagen, Denmark

³ Niels Bohr Institute, University of Copenhagen, Jagtvej 128, 2200 Copenhagen N, Denmark

⁴ Department of Physics, University of Warwick, CV4 7AL Coventry, United Kingdom

⁵ DARK, Niels Bohr Institute, University of Copenhagen Jagtvej 128, 2200 Copenhagen N, Denmark

⁶ Artemis, Université Côte d'Azur, Observatoire de la Côte d'Azur, CNRS, F-06304 Nice, France